Geoscience Frontiers 13 (2022) 101290

HOSTED BY

Contents lists available at ScienceDirect

Geoscience Frontiers

journal homepage: www.elsevier.com/locate/gsf

Research Paper

Mass balance and morphological evolution of the Dokriani Glacier, central Himalaya, India during 1999–2014

Purushottam Kumar Garg [a,b,*], Jairam Singh Yadav [b], Santosh Kumar Rai [b], Aparna Shukla [b,c]

[a] Indian Institute of Technology Indore, Khandwa Road, Simrol, Indore 453552, India
[b] Wadia Institute of Himalayan Geology, 33, GMS Road, Dehradun 248001, India
[c] Ministry of Earth Sciences, Prithvi Bhavan, Lodhi Road, New Delhi 110003, India

ARTICLE INFO

Article history:
Received 14 April 2021
Revised 24 July 2021
Accepted 22 August 2021
Available online 25 August 2021
Handling Editor: C.J. Spencer

Keywords:
Glacier mass balance
Debris cover
Epiglacial morphology
Supraglacial channel
Dokriani Glacier
Central Himalaya

ABSTRACT

Glaciological mass balance (MB) is considered the most direct, undelayed and unfiltered response of the glaciers to climatic perturbations. However, it may inherit errors associated with stake under-representation, averaging over the entire glacier and human bias. Therefore, proper validation of glaciological MB with geodetic MB is highly recommended by the World Glacier Monitoring Service (WGMS). The present study focuses on the Dokriani Glacier, central Himalaya which is one of the bench-mark glaciers in the region and has glaciological MB records from 1993 to 2013 with intermittent gaps. In the present study, firstly the glaciological MB series is extended to 2014 i.e., field-based MB for one more year is computed and, to compare with it, the geodetic MB is computed for the 1999–2014 period using high resolution Cartosat-1 digital elevation model (DEM) and SRTM DEM. Finally, the study assesses the regional representation of the Dokriani Glacier in terms of MB and evaluates the influence of the MB regime on its morphological evolution. Results show that the average glaciological MB (-0.34 ± 0.2 m water equivalent (w.e.) y^{-1}) is more negative than the geodetic MB (-0.23 ± 0.1 m w.e. y^{-1}) for the 1999–2014 period. This is likely because of the partial representation of glacier margins in the glaciological MB, where melting is strikingly low owing to thick debris cover (>30 cm). In contrast, geodetic MB considers all marginal pixels leading to a comparatively low MB. A comparative assessment shows that the MB of Dokriani Glacier is less negative (possibly due to its huge accumulation area) than most other glacier-specific and regional MBs, restricting it to be a representative glacier in the region. Moreover, continuous negative MB has brought a peculiar change in the epiglacial morphology in the lower tongue of the glacier as differential debris thickness-induced differential melting has turned the glacier surface into a concave one. This concavity has led to development of a large (10–20 m deep) supraglacial channel which is expanding incessantly. The supraglacial channel is also connected with the snout wall and accelerates terminus disintegration. Given the total thickness of about 30–50 m in the lower glacier tongue, downwasting at its current pace, deepening/widening of supraglacial channel coupled with rapid terminus retreat may lead to the complete vanishing of the lower one km glacier tongue.

1. Introduction

Glaciers all over the world have undergone substantial mass loss at least since middle of the last century with varied pace of mass wastage rate (Zemp et al., 2015; WGMS, 2017). However, exceptions are there with only a few regions such as the Karakoram, Pamir and western Kunlun which remained almost balanced (Gardelle et al., 2013; Brun et al., 2017; Zhou et al., 2018). The declining glaciers have strong bearing on regional water supply (Barnett et al., 2005), sea level rise (Chen et al., 2013) and natural hazards (Huggel et al., 2004; Kääb et al., 2005), warranting their frequent and regular monitoring. Glaciological glacier mass balance (MB) is most direct parameter of glacier monitoring which represents an undelayed and unfiltered response of a glacier system to seasonal/annual meteorological conditions as well as to long term climate change (Azam et al., 2018; Kumar et al., 2021). However, field based MB is limited to only 26 glaciers in the entire Himalayan region (Azam et al., 2018; Soheb et al., 2020; Angchuk et al., 2021) including 17 glaciers in the Indian Himalayan region (IHR). Further, most of the MB series in the Himalaya are limited

* Corresponding author at: Indian Institute of Technology Indore, Khandwa Road, Simrol, Indore 453552, India.
E-mail address: garg.glacio@gmail.com (P.K. Garg).

https://doi.org/10.1016/j.gsf.2021.101290
1674-9871/

to <10 years and, hence, cannot be used as reference glaciers for which >30 observation years are needed.

The glaciological MB method is primarily based on in situ stakes and pit measurements over representative points which are interpolated (between measured points) and extrapolated (to unmeasured regions) to have glacier wide coverage (Cogley et al., 2011; Zemp et al., 2013). The representativeness of these points and the method used for interpolation/extrapolation (e.g. kriging, contour, profile) form the major sources of systematic errors in glaciological MB estimations (Hock and Jensen, 1999; Pelto, 2000; Zemp et al., 2013). Therefore, it is highly recommended that glaciological MB series are homogenized (i.e. validated and calibrated) with decadal geodetic balances for common survey period in order to model and remove the systematic biases which lead to disagreements between measured and true values (Cogley et al., 2011; Zemp et al., 2013). Despite of coarse resolution, geodetic method is advantageous as it provides spatially distributed MB even in inaccessible areas. However, prior to homogenization, rigorous uncertainty estimations of both the methods is mandatory. Zemp et al. (2013) suggested that homogenization process needs to become a 'standard procedure' for every MB program. Such exercises have been carried out at several glaciers of the world (Thibert et al., 2008; Huss et al., 2009; Andreassen et al., 2012) including a few glaciers of the Himalaya (Nuimura et al., 2011; Vincent et al., 2013; Pieczonka and Bolch, 2015; Berthier et al., 2016). Azam et al. (2018) highlighted that harsh conditions of the Himalayan region limit the number of point accumulation measurements; therefore, it becomes even more crucial to check the biases in glaciological MB series. However, most of the available glaciological MB series in the Himalaya, particularly in IHR, have never been validated/calibrated with the geodetic one (Azam et al., 2018).

The Himalaya is one of the worst affected regions by climate change where temperature rise has exceeded the world average (INCAA, 2010; Bolch et al., 2012; IPCC, 2013) leading to a significant and accelerated decline in the Himalayan glaciers (Kääb et al., 2012; Gardelle et al., 2013; Brun et al., 2017). This is manifested with the MB rates of −0.22 ± 0.13 m w.e. during 1975–2000 which have almost doubled to −0.43 ± 0.14 during 2000–2016 (Maurer et al., 2019). The continuous mass loss has led to glacier slowdown (Azam et al., 2012; Tiwari et al., 2014; Garg et al., 2017a; Dehecq et al., 2019), concomitant debris growth in ablation zone of glaciers (Shroder et al., 2000; Scherler et al., 2011; Garg et al., 2017b) and changes in the epiglacial morphology (Quincey et al., 2009; Benn et al., 2012; Garg et al., 2021). These morphological evolutions need due attention in order to understand current status as well as future response of a glacier system to different forcing factors.

The present study focuses on the Dokriani Glacier, central Himalaya which in one of the well monitored glaciers in terms of glaciological MB, glacier thickness, air temperature variability, surface elevation changes, debris cover influence, snout retreat and surface morphology (Gergan et al., 1999; Dobhal et al., 2008; Dobhal and Mehta, 2010; Pratap et al., 2015; Azam et al., 2018; Yadav et al., 2019; Yadav et al., 2020). Glaciological MB measurements on this glacier first started in 1993 and available since then upto 2013 with intermittent gaps (Pratap et al., 2016). Here, considering the above discussed constrains, the major objectives of the paper are to:

- extend glaciological MB of the Dokriani Glacier up to 2014.
- estimate geodetic MB for 1999–2014 period and validation of glaciological MB with that of geodetic one for this common survey period.
- assess regional representativeness of the Dokriani Glacier MB.
- understand morphological evolution of the glacier during the study period.

In-situ (2013/14) and satellite remote sensing data (2000–2014) have been utilized to quantify the MB and assess the morphology of the glacier. Further, the paper has been organized into several sections. First, a concise description of the study area is given followed by the details of data and methodology used. Then, results of glaciological and geodetic MB are given. Finally, comparison of results with previous studies, regional representativeness and morphological changes of glacier are presented followed with conclusions.

2. Site description

The Dokriani Glacier (snout coordinates: 30.86°N, 78.79°E) is located in the Bhagirathi basin of the central Himalaya, lying ~40 km (aerial distance) from Uttarkashi town of Uttarakhand, India. Its meltwater forms Din Gad stream which contributes to the Bhagirathi River. The glacier has two accumulation areas- first on the north slope of Draupadi ka Danda peak (5716 m asl), and second on the western slope of Janoli peak (6632 m asl) (Fig. 1). Based on 2014 Landsat image, total area of the Dokriani Glacier is 6.34 ± 0.16 km^2 with a total length of 5.75 ± 0.06 km (Garg et al., 2017b). Accumulation area of the glacier is quite wide (~2.5 km) with strikingly narrow lower ablation portion (~80 m) which is constrained between 40 and 60 m elevated lateral moraines (Dobhal et al., 2004). The glacier snout is well defined and located at 3869 m asl (Garg et al., 2017b). As per recent estimates (2014), ~18% of the total glacier area is covered by debris. The central portion (along center flowline) of glacier is either clean or have very thin debris cover (<2–5 cm) whereas towards margins the debris thickness reaches upto 25–40 cm (Pratap et al., 2016). The debris is of schist and gneiss/granite origin which ranges in size from fine grain silt to boulders exceeding several meters (Fig. 2). Various morphological features such as ogives, crevasses, moulin and supraglacial channels are well-developed on the glacier (Dobhal et al., 2008; Dobhal and Mehta, 2010).

3. Data and methods

3.1. Glaciological mass balance measurement

The field-based (glaciological) MB of the Dokriani Glacier is available since 1993 upto 2013 (Dobhal et al., 2008; Pratap, 2015; Pratap et al., 2016). The present work is an attempt to validate the glaciological MB for the period after 1999 using the geodetic one. For post-1999 period, the glaciological MBs are available for 2000 and 2008–2013 (Dobhal et al., 2008; Pratap, 2015). We add the glaciological MB for one more year i.e., for 2014 with complete details of methodology as follows.

3.1.1. Ablation measurement

To observe the surface ablation of the Dokriani Glacier (2013/14), a network of 28 ablation stakes was drilled over the glacier surface using steam-driven ice drill machine along the different altitudinal zones (3995–5000 m asl) at the end of ablation season, i.e., in the end of October 2013 (Figs. 1 and 2). The stakes were set up as per established methodology (Østrem and Brugman, 1991; Dobhal et al., 2008, 2013; Cogley et al, 2011). Considering the discrete surface conditions, dense network was put in the lower ablation zones, while the smaller number of stakes were installed in the upper ablation zones (Fountain and Vecchia, 1999) (Fig. 1). Thus, each stake situated at every 100 m elevation could be representative of debris-covered and debris-free zones. The exposed length of each stake was measured for every 15 days interval throughout the summer period following the international

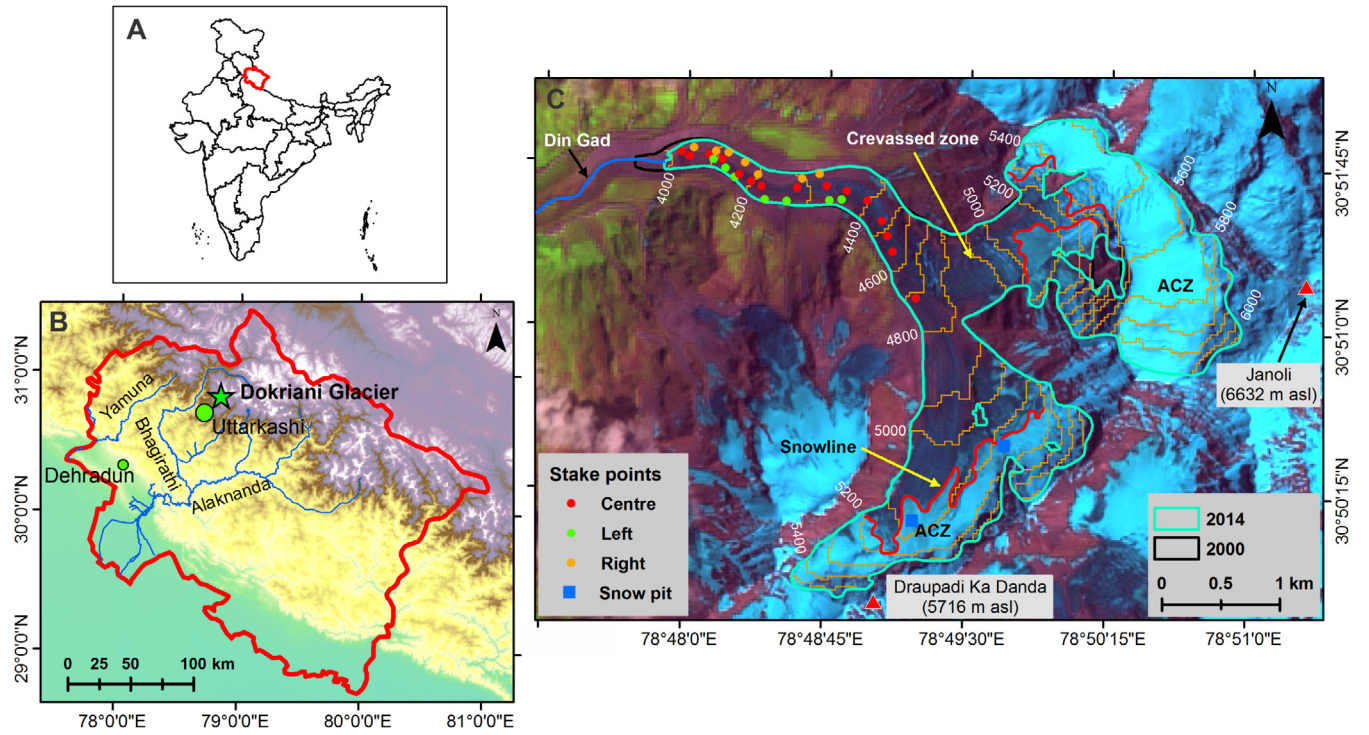

Fig. 1. Location map of the Dokriani Glacier (A and B). Temporal glacier boundaries in Panel (C) show a clear terminus retreat during 2000–2014. Supraglacial debris (SGD) is also identifiable in the lower ablation zone. Notice huge accumulation zone (ACZ) of the glacier. Ablation stake networking on the glacier during October 2013 is shown in Panel (C). The stakes were set up as per methodology proposed by several researchers (Østrem and Brugman, 1991; Dobhal et al., 2008, 2013; Cogley et al, 2011). The lower portion has denser network of stakes to cover the spatial heterogeneity in the melting. The snowline shown on Panel (C) is for the year 2014 and obtained from Garg et al. (2017b). Background image shown in the panel (C) is a pan-merged Landsat Enhanced thematic mapper plus (ETM+) image of 20 August 2014.

norms (Østrem and Brugman, 1991; Cogley et al., 2011). The winter ablation was computed using cumulative melt between October and March whereas the annual ablation was based on the summation over the summer and winter ablations. The net monthly ablation in water equivalent unit was estimated using following relation as Eq.(1):

$$\boldsymbol{A_t = L_e * \rho_{Avg}} \quad (1)$$

where, A_t = net monthly ablation in water equivalent (w.e.); L_e = exposed length of stakes; $\boldsymbol{\rho}$ = average ice density (i.e, ~0.85 g m^{-3} in the ablation zone for Dokriani Glacier; Pratap, 2015).

3.1.2. Accumulation measurement

Accumulation occurring over the glacier surface is mainly contributed and regulated through the solid precipitation, snow avalanches, and drifting of snow by wind. Generally, in the summer season, occasional solid precipitation was identified in the accumulation zone of Dokriani Glacier and, therefore, only residual accumulation was estimated at the end of October month. The residual snow depth was estimated by digging the snow pits (Fig. 2) nearby the central line of the accumulation zone where avalanche and snow drifting by wind are found to be minimal (Fig. 1). Estimated snow depth was further extrapolated to obtain snow depth at several elevation bands in the upper reaches of Dokriani Glacier. Multiplying the snow depth of these bands with measured average snow density 560 ± 40 kg m^{-3} (Dobhal et al., 2008; Pratap, 2015) provided the accumulation amounts in meter water equivalent (m w.e.) (Fig. 2).

3.1.3. Annual glaciological mass balance computation

The annual accumulation was computed by multiplying snow depth (in m w.e.) with area corresponding to each elevation band determined from Shuttle Radar Topographic Mission Digital Elevation Model version-3 (SRTM DEM-v3). The annual MB of Dokriani Glacier was estimated using following Eq.(2):

$$B_a = C_a - A_a \quad (2)$$

where, C_a and A_a are the annual accumulation and annual ablation (conventionally, both are taken as positive), respectively. B_a is essentially the annual change in the volume of the glacier, which was converted into m w.e. by multiplying with the density factor (Dobhal et al., 2008; Pratap, 2015). The specific MB (B_s) was obtained by averaging the annual MB over the area of the glacier as given in the Eq. (3):

$$B_s = \frac{1}{S}\iint b_n ds \quad (3)$$

where b_n is net surface mass balance and S is the total surface area of glacier.

3.2. Geodetic mass balance estimation

For geodetic MB estimations, the SRTM DEM-v3 having 1-arc second resolution (30 m spacing) was acquired for the study area from USGS Earth Explorer website (https://earthexplorer.usgs.gov/). The SRTM provides horizontal and vertical accuracy of 20 m and 10 m, respectively. Then, high resolution and snow-free Cartosat-1 stereo-pair (19 November 2014) was procured from National Remote Sensing Centre, India (https://www.nrsc.gov.in). For hilly terrain, accuracy of Cartosat-1 DEM is reported to be in order of ~4–8 m in vertical and ~15 m in horizontal direction (Ahmed et al., 2007; Muralikrishnan et al., 2013) which makes it suitable for cryospheric studies (Bolch et al., 2011; Agarwal et al., 2017; Bhushan et al., 2017). The detailed steps for geodetic MB computations are discussed in following sub-sections.

Fig. 2. Steam drill operation (panels (A) to (D)) for ablation stake networking on the Dokriani Glacier during October 2013. Panels (E) and (F) show snow pitting in the accumulation zone. The stakes were set up as per methodology proposed by several researchers (Østrem and Brugman, 1991; Dobhal et al., 2008, 2013; Cogley et al, 2011).

3.2.1. DEM preparation

The Rational Polynomial Coefficients (RPC), provided along with Cartosat-1 data, were used to generate DEM from the stereo-pair without ground control points (GCP). The RPCs are real time calculated based on the position of the satellite at the time of image acquisition and have high fitting accuracy (Ahmed et al., 2007). Though, GCPs can be used to improve the correlation between the image pair, they need to be well-distributed and two to three times more accurate than the spatial resolution of image (Agarwal et al., 2017). To achieve the proper overlapping of the stereo-pair, a total number of 127 well-distributed tie points were collocated and the overall image RMSE was minimized to <2 pixels after several iterations. Finally, the DEM was extracted in 30 m spacing with region strategy set to high mountains and geocoded in the Universal Transverse Mercator (UTM) World Geodetic System 1984 (WGS84) Zone 44 North.

3.2.2. Horizontal coregistration

Prior to comparison on the pixel to pixel basis, temporal DEMs must be coregistered (Nuth and Kääb, 2011). Here, the SRTM DEM-v3 was taken as a reference DEM and Cartosat-1 DEM was coregistered to it. The congruence between the two DEMs was achieved by minimizing the standard deviation of elevation difference over glacier free stable terrain (Fig. 3). The least error prone stable ground pixels were obtained by (a) masking glaciated region using Global Land Ice Measurement from space (GLIMS) glacier outlines, (b) excluding slope <4° and >45° and (c) removing elevation difference outliers (i.e. ± 100 m) (Berthier et al., 2016; Garg et al., 2019). Statistics of pre-and post-coregistration of Cartosat-1 DEM relative to SRTM DEM-v3 are given in Table 1.

3.2.3. Vertical biases correction

Various vertical biases potentially affecting the elevation difference between the two DEMs were carefully checked and corrected using all the reliable pixels over the stable terrain (Fig. 3; Table 1). Here, in addition to above discussed masks, the outlier mask was further narrowed down to ± 50 m (roughly 3 times of standard deviation; Table 1). First, we correct for along/cross track biases which can be introduced by anomaly in the attitudes (roll, pitch or yaw) of the satellite. The azimuth of Cartosat-1 ground track

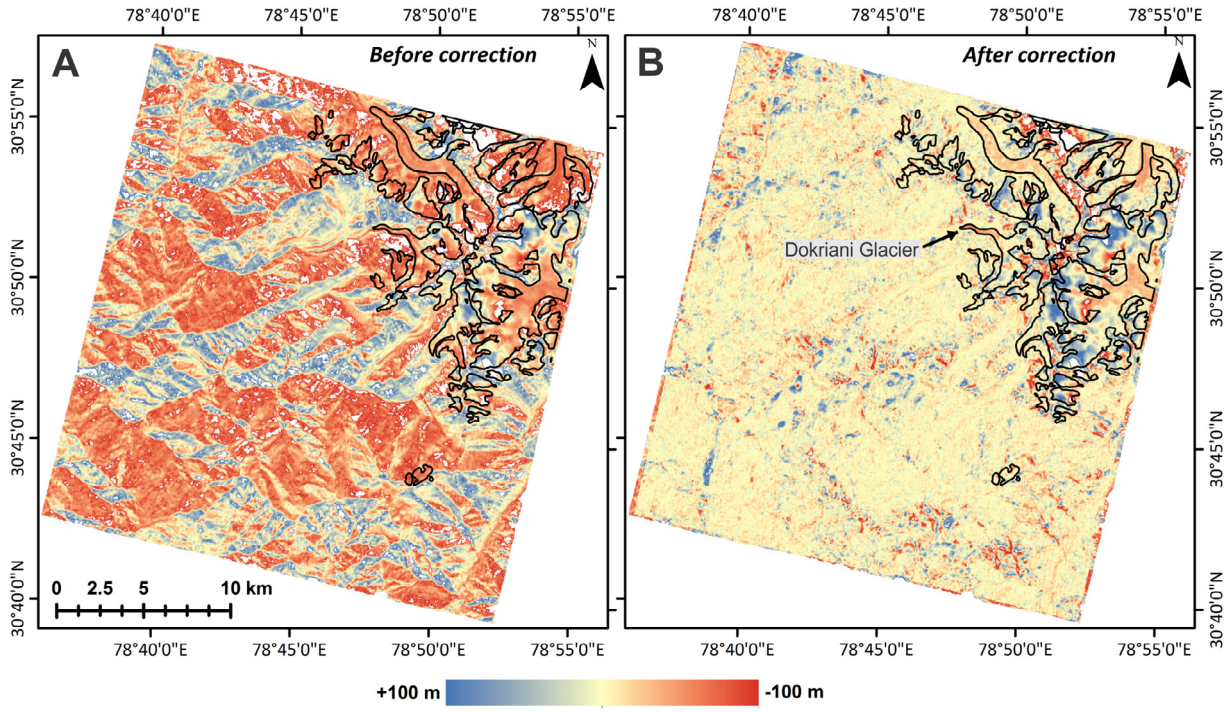

Fig. 3. Map showing before (A) and after adjustment (B) elevation difference images deduced by differencing 2000 SRTM DEM from 2014 Cartosat 1 DEM. Various corrections include 3-D coregistration, along/across track, elevation, slope and terrain curvature related error corrections. A good congruence between the temporal DEMs can be seen on stable terrain (mean difference = −0.02 m y^{-1}). The black polygons show the GLIMS glacier boundaries.

Table 1
Statistics of the elevation differences on the non-glaciated terrain for the raw and corrected difference images. The corrections 1–5, respectively denotes the 3-D coregistration, along/across track, elevation, slope and terrain curvature related error corrections. The improvement in standard deviation (SD) shows the improvement after each correction compared to the previous step.

SRTM-Cartosat 1 (non-glaciated terrain)	Raw	Corr. 1	Corr. 2	Corr. 3	Corr.4	Corr.4
Mean (m)	−31.49	−0.45	0.35	0.07	−0.35	−0.02
Standard deviation (m)	20.31	15.84	10.71	10.49	10.50	10.10
Improvement in SD (%)	–	21.97	42.42	2.08	−0.12	3.81

was used to rotate the coordinate system followed by the computation of elevation difference along and cross track over the stable terrain and then biases were corrected using high order polynomial (Berthier et al., 2007; Nuth and Kääb, 2011; Gardelle et al., 2013). The SRTM DEM is reported to have systematic biases as a function of altitude (Berthier et al., 2007). In our study area, we plotted the elevation difference over stable terrain as a function of altitude and used sixth order polynomial to correct the bias. Subsequently, slope and aspect dependent biases were also detected and corrected using high order polynomial functions. The difference in spatial resolution of the two DEMs may result in elevation-implicit bias in mountainous terrain (Gardelle et al., 2013) which were checked and corrected using relationship between the maximum curvature and elevation difference over stable areas. All the corrections have resulted in an overall improvement of 50.27% in the standard deviation of elevation difference (Fig. 3).

3.2.4. C-band penetration and seasonality correction

DEMs derived by SAR-interferometry are potentially biased by penetration effects of the radar waves into ice and snow and hence, might reflect some lower surface than the actual glacier surface (Rignot et al., 2001; Gardelle et al., 2012; Zhou et al., 2018). The SRTM DEM in C-band have varying capability of penetration (ranging from 0 to 10 m; Gardelle et al., 2012) in different glacier facies (e.g. snow, ice, debris), with varying physical and dielectric properties (Agarwal et al., 2017; Zhou et al., 2018). Kääb et al. (2012) computed penetration values by extrapolating elevation difference trends derived from Ice Cloud and Elevation Satellite (ICESat) measurements to 2000 for several sub-regions in High Asia. For our study region (i.e. Uttarakhand), they reported penetration values to be 2.3 ± 0.6 m, 1.7 ± 0.6 m and 0.4 ± 0.8 m for firn/snow, clean ice and debris-covered ice, respectively. However, classifications of regions by Kääb et al. (2012) were very broad and they combined Himachal Pradesh, Uttarakhand and West Nepal in a single region. Recent studies have calculated penetration depth values by comparing the SRTM C-band with simultaneously acquired SRTM X-band data which vary from region to region (Gardelle et al., 2013; Vijay and Braun, 2016; Agarwal et al., 2017; Zhou et al., 2018). For the proximity to our study area i.e., central Himalaya, Gardelle et al. (2013) reported a penetration value of 1.9 m (average for Bhutan and Everest region). Zhou et al. (2018) also calculated penetration values of 1.9 m for the nearby western Nepal region. Recently, Bandyopadhyay et al. (2019) have estimated an average penetration depth value of 3.5 m dedicatedly for the Uttarakhand region. In the present study, we have used C-band penetration depth values of 3.5 m for snow/ice as suggested by Bandyopadhyay et al. (2019) for our study area, and 0.4 ± 0.8 m for debris-covered ice as suggested by Kääb et al. (2012). To distinguish among the various facies, we have adopted the classification

from Garg et al. (2017b) and applied the penetration correction to each pixel belonging to particular facie separately.

Seasonality bias is introduced in elevation difference calculations when the two DEMs are acquired in different months (Gardelle et al., 2013; Vincent et al., 2013). The SRTM DEM is acquired during February2000 and the Cartosat-1 DEM that we used in the present study is of November 2014. Therefore, possible mass change during these winter months (i.e. November-February) needs to be considered to make both the dataset comparable. In the present study we have applied a seasonality correction value of 0.1475 m w.e. per winter month which is based on average accumulation rate measured for the Dokriani Glacier on field by the present study and Pratap (2015). This value compares well with mean value of winter MB (0.15 m w.e. per month) of 35 glaciers of Northern Hemisphere (Ohmura, 2011; Gardelle et al., 2013).

3.2.5. Outlier/data gap removal and mass balance calculation

The elevation change over entire glacier is not homogenous and varies with altitude following a non-linear trend. For a glacier with negative MB, maximum and minimum down wasting will typically occur at snout region and higher altitudes (i.e. accumulation region), respectively (Schwitter and Raymond, 1993). This phenomenon requires different thresholds to be applied while filtering outliers in the accumulation and ablation zones (Pieczonka and Bolch, 2015; Zhou et al., 2018). Here, we used an approach proposed by Zhou et al (2018) to determine maximum allowable thickness change (Δh_{max}) at certain altitude which is a simplified version of the 'sigmoid approach' presented by Pieczonka and Bolch (2015), as Eqs.(4) and (5).

$$E_{\text{norm}} = \frac{E_{\max} - E_{\text{glacier}}}{E_{\max} - E_{\min}} \tag{4}$$

$$\Delta h_{\max} = A * E_{\text{norm}} \tag{5}$$

where, $E_{\max}$ and $E_{\min}$ are the maximum and minimum glacier elevation, E_{glacier} is elevation of individual glacier pixel, and A is the empirical coefficient which represents the maximum elevation change at the glacier front. Here, for the Dokriani Glacier a value of −60 m has been chosen based on field measurements (Dobhal et al. 2008; Pratap et al. 2015) along with earlier reported geodetic observations (Dobhal and Mehta 2010; Bandyopadhyay et al., 2019). The missing and discarded values using $\Delta h_{\max}$ were replaced by the mean values of the respective 100 m elevation band. In the next step, area-weighted mean of elevation change for each 100 m altitude band was calculated. Finally, the mass budget for the Dokriani Glacier was determined using the average densities of 850 ± 60 kg m^{-3} and 560 ± 40 kg m^{-3}, respectively for ice and snow/firn as measured in the field on this glacier (Dobhal et al. 2008; Pratap, 2015).

3.3. Uncertainty estimation

Quantification of uncertainties is essential for substantiating results of any study and thus aiding proper interpretation and resolutions. Previously reported error in the surface MB series data by glaciological method lies between ±0.2 and ±0.4 m w.e. (Cogley and Adams, 1998; Braithwaite et al., 1998; Jansson, 1999; Cox and March 2004; Kumar et al., 2021). We have considered various roots which introduce errors in the MB measurements. The movement of the Dokriani Glacier was very slow (average velocity: 10.53 m y^{-1} in 2015) (Shukla et al., 2018). Therefore, error linked due to this factor may be negligible. Mechanical error like joints, tilting of stakes, inexact choice of bottom surface of stakes, emergence of stakes by filling of water in the hole during extreme melting have been seriously taken into account in the MB measurement. These issues were attempted to minimize by averaging the results of large number of stakes installed over the glacier surface. Further, error raised due to temporal variation of the glacier area was reduced by demarcating the area of the most recent image of the Dokriani Glacier. The errors occurred due to stake height measurement, density and snow/ice depth measurement contribute major uncertainty in the MB measurement. The total error in these points' measurement is estimated as ±0.21 m w.e., which is comparable to other MB studies in the IHR (Azam et al., 2018). Density and depth measurement in the accumulation area may introduce hidden error and were tried to rectify by taking careful measurement while doing field visit.

The uncertainty in geodetic MB was quantified using sequential steps. In order to quantify vertical accuracy, we have considered all the pixels over stable terrain with slope less than or equal to 45° (~1.2 million pixels). The standard deviation of the elevation difference in stable terrain ($\underline{\delta_{si}}$) was used to approximate the error in elevation change computations (δ_i) for each 100 m altitude band (Gardelle et al., 2013; Zhou et al., 2018) using Eqs. (6) and (7).

$$\delta_i = \frac{\delta_{si}}{\sqrt{N_e}} \tag{6}$$

$$N_e = \frac{N_t * R}{2d} \tag{7}$$

where N_t and N_e are the total and effective observations, respectively. R represents pixel resolution and d is the distance of autocorrelation which is equal to the range of influence of the obtained modelled spherical semi-variogram for elevation change values on stable terrain and is equal to 600 m (Bhushan et al., 2018; Zhou et al., 2018). In the next step, overall uncertainty in glacier elevation change (δ_{gi}) was computed taking into account the penetration uncertainty (δ_p) of 1.5 m (i.e. 50% of the value applied for penetration correction) using Eq. (8). Finally, the mass budget uncertainty (δ_{mb}) were quantified as per Eq. (9).

$$\delta_{gi} = \sqrt{(\delta_i)^2 + (\delta_p)^2} \tag{8}$$

$$\delta_{mb} = \sqrt{\left(\frac{\delta_{hi} * \delta_\rho}{t * \rho_w}\right)^2 + \left(\frac{\delta_{gi} * \rho_i}{t * \rho_w}\right)^2} \tag{9}$$

where δ_{hi} is the observed thickness changes over glacier, δ_ρ is the uncertainty in density estimates (i.e. ±60 kg m^{-3}), ρi is the density of ice used in the present studys (i.e. 850 ± 60 kg m^{-3} for ice and 560 ± 40 kg m^{-3}, for snow/firn), ρ_w is the density of water (i.e. 1000 kg m^{-3}) and t is the time period (i.e. 15 years).

4. Results

4.1. Glaciological mass balance of the Dokriani Glacier for 2014

Ablation area of the Dokriani Glacier is enclosed between well-elevated right lateral and left lateral moraines (Fig. 1). The ablation zone is covered by debris of varying thickness (Pratap et al., 2015), which was limited in the elevation range of 4000–4400 m asl, whereas clean ice areas is found from 4400 to 5000 m asl. However, most of the areas around central flowline of the glacier are debris free (Fig. 1). The observed melting rate for 2013/14 reflects the distinct pattern in ablation and accumulation period, as well as varies along the altitudes and with the dimension of debris. Results reveal that the rate of surface ablation (−1.8 to −6.3 m w.e.) significantly varied within the elevation bands with maximum near the snout (Fig. 4). Ablation stakes along central line showed higher surface melting (>4.0 m w.e.) while stakes nearby the lateral moraines had lower surface melt (<2.0 m w.e.). Conversely, change in accumulation along elevations was almost constant. Equilibrium line

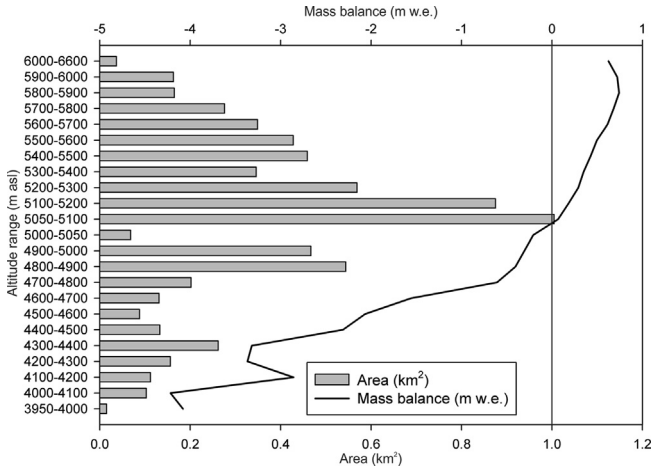

Fig. 4. Specific mass balance for the year 2013/14 versus elevation and area distribution of the Dokriani Glacier derived from field measurements (stakes and pits). Notice a higher ablation below 4400 m asl owing to the presence of a supraglacial channel.

altitude (ELA) was established by drawing a relationship between the MB and altitudes to be ~5055 m asl resulting in the area accumulation ratio (AAR) of 0.682 (Fig. 4). The annual MB of the Dokriani Glacier was estimated to be −0.29 ± 0.21 m w.e. for the year 2013/14.

4.2. Geodetic mass balance of the Dokriani during 1999–2014

The study conducted for the period of 2000–2014 indicates that the Dokriani Glacier underwent significant thinning particularly in the lower ablation tongue. It may be noted that after applying seasonality corrections, the SRTM DEM represents the glacier surface of ablation period of the year 1999 making total period of study to be 15 years. During this 15 year period, the average glacier-wide thinning was −10.13 ± 1.82 m (or −0.68 ± 0.12 m y^{-1}). The highest lowering (average of altitude bands) of −38.63 ± 1.57 m (−2.58 ± 0.10 m y^{-1}) was observed at the altitude band 4100–4200, followed by −38.21 ± 1.58 m (−2.55 ± 0.11 m y^{-1}) at 4000–4100 m (Fig. 5). Notably, much higher surface lowering was observed along the central flow line of the glacier (maximum up to 53.73 ± 1.82 m), which made a linear pattern upto one km distance from the snout (Fig. 5). Interestingly, margins showed low surface lowering. The surface lowering was dominant up to 2.5 km distance from the snout which constitutes the narrow ablation tongue of the glacier. Ahead of this there was no uniform pattern and the surface elevation change was very less in magnitude. The accumulation zone has shown minimal change and remained relatively stable during the study period of 15 years. Finally, after

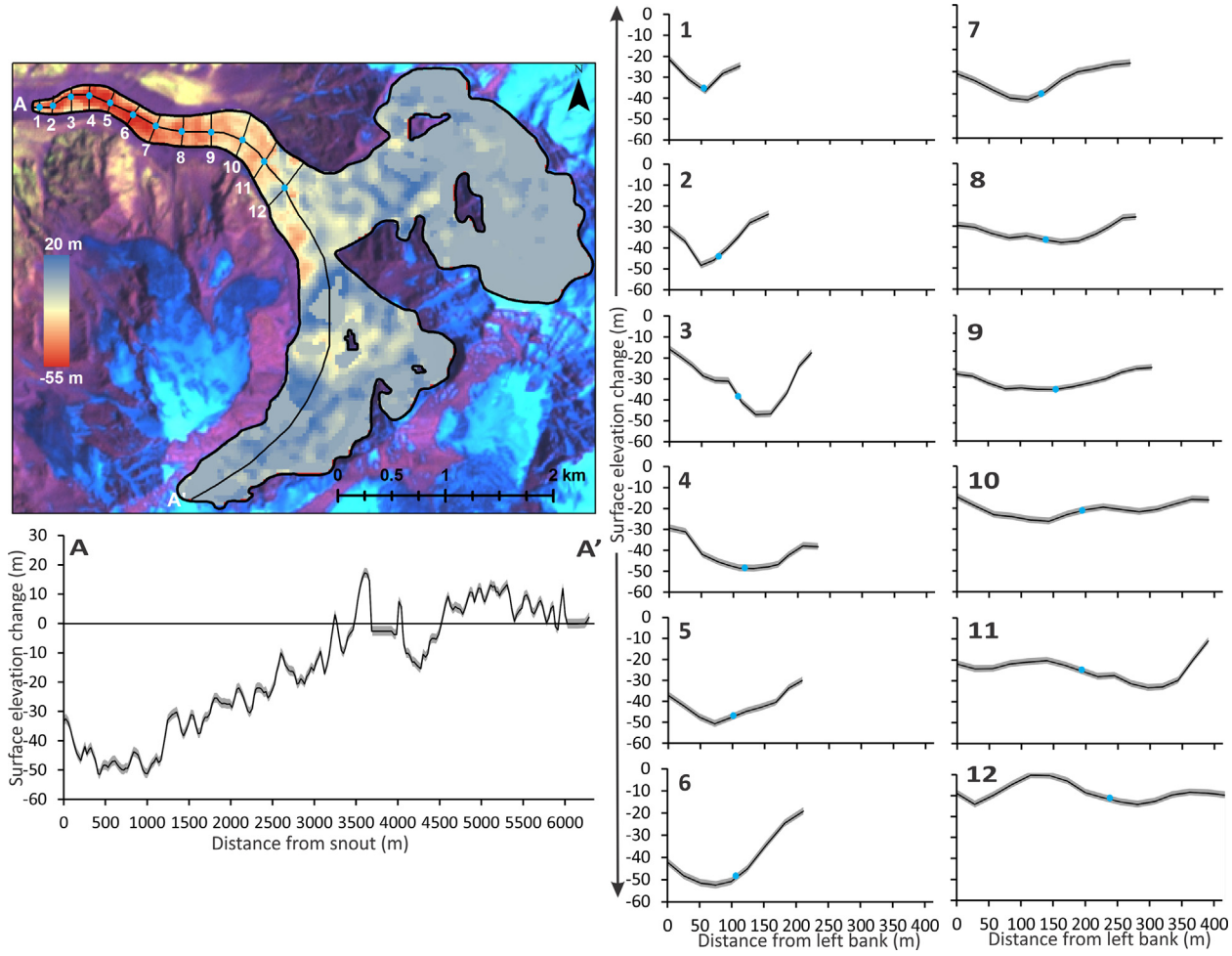

Fig. 5. Surface elevation change profile on the Dokraini glacier between 1999 and 2014 along the central flow line (A–A') and across different profiles (1–12). Notice a clear deepening in central portion of the glacier which indicates presence of a supraglacial channel. The supraglacial channel initiates from profile 8 (about 1.5 km distance upglacier from the snout) and continues upto the snout but gradually becomes narrow and deep. Above profile 8, the glacier experiences almost uniform downwasting across the width. Blue dots on the map show intersection of cross profiles and central flow line.

applying the seasonality correction, the geodetic MB of the Dokriani Glacier equals −3.48 ± 1.35 m w.e. during 1999–2014 which corresponds to the specific MB of −0.23 ± 0.1 m w.e. y^{-1}.

5. Discussion

5.1. Understanding glaciological and geodetic mass balance of the Dokriani Glacier

The Dokriani Glacier has been monitored for glaciological MB since 1993 and, inspite of intermittent gaps, it has one of the longest records of field based MB measurements in the IHR (Pratap et al., 2016; Azam et al., 2018). Results reveal that below 4200 m asl glacier experienced a greater mass loss due to calving of ice near the snout position. The MB decreases almost with a constant rate above the elevation 4400 m. This change may be attributed to presence of clean ice and gentle slope. Elevation zone 5000–5100 covering the largest area evinces least ablation. This may be controlled by temperature effect with altitudes (Pratap et al., 2015).

Results of field and geodetic measurements validate each other in terms of spatial variation of downwasting. A relatively higher downwasting at 4000–4100 m asl altitude band is well evident with elevated values along the central flowline in the ablation stake and geodetic measurements. The field-based MB ranges from −0.24 m w.e. y^{-1} in 2011 to −0.46 m w.e. y^{-1} in 1999 leading to an average of −0.34 m w.e. y^{-1} during 1999–2014. It is notable that there is a large gap of 7 years (2001–2007) in glaciological measurements which restricts interpolation of MB values for gap years. In this context, geodetic MB is not only useful in validating the long-term glaciological MB series but it also gives an idea about the magnitude of change representing the gap years. The geodetic results show that the MB of the glacier was −0.23 ± 0.1 m w.e. y^{-1} during 1999–2014 which, though follow the similar negative trend (Fig. 6), are less negative than the glaciological MB (−0.34 m w.e. y^{-1}) (Fig. 6). The glaciological MB involves interpolation of the stake points over different altitude bands which makes capturing spatial variability challenging (Zemp et al., 2015; Azam et al., 2018). The major hindrance in the stakes measurement is that (a) inaccessible glacier areas (e.g. heavily crevassed) often remained unsampled and (b) stakes are seldom installed in the extreme glacier margins. In debris-covered glacier margins, melting is usually low as compared to central portion of the glacier owing to typical debris thickness distribution pattern which insulates the undelaying ice (Nicholson and Benn, 2006; Anderson and Anderson, 2018).

In case of the Dokriani Glacier, despite a dense network of ablation stakes in the lower ablation tongue, only a few stakes could be installed in the extreme margins. From spatial distribution of the geodetic MB, it is apparent that the down wasting is remarkably higher in the central portion of the glacier than that in margins (Fig. 5). Thus, a tenuous representation of margins in the glaciological MB would have probably led to relatively more negative MB. Contrarily, the geodetic MB includes margin pixels where less melting occurred. Moreover, some boundary pixels may represent transition between glacier and non-glacier area and, hence, show low average elevation change (Fig. 5) leading to less negative geodetic MB. A recent study by Azam and Srivastava (2020) have reconstructed the MB of the Dokriani Glacier for 1979–2018 period and reported an average MB of −0.25 m w.e y^{-1} (Fig. 7) which is consistent with the geodetic measurement presented in this study. However, Azam and Srivastava (2020) reported a large variability on the decadal scale. They found that the glacier was in almost stable condition during 1989–1997 with MB of –0.02 m w.e. y^{-1}. However, for 1998–2006 and 2007–2018 periods the MBs were −0.28 m w.e. y^{-1} and −0.33 m w.e. y^{-1}, respectively, showing an increase in mass loss rates. These values are in line with glaciological MB and validate them.

5.2. Comparison of mass balance of the Dokriani Glacier and other mass balance series across the Himalayan region

There are 26 Himalayan glaciers which have been surveyed for glaciological MB (Pratap et al., 2016; Azam et al., 2018; Supplementary Data, Table S1) at varying time periods. Considering average MB of all glaciers, the MB of Dokriani Glacier is less negative than 70% glaciers (i.e.18 glaciers) (Supplementary Data, Table S1).

In the central Himalayan region limited to IHR, only 4 glaciers have been surveyed for the glaciological MB namely the Tipra Bank (1981–1988; −0.14 m w.e. y^{-1}), Dunagiri (1984–1990; −1.04 m w.e. y^{-1}), Chorabari (2003–2010; −0.73 m w.e. y^{-1}) and Dokriani (1993–2014; −0.32 m w.e. y^{-1}) (Fig. 6). The MB of the Dokriani has been more negative than the Tipra Bank but considerably less negative than the Dunagiri and Chorabari glaciers (Fig. 6). Moreover, a few studies have estimated the MB of Uttarakhand glaciers on the regional scale as well as on individual glacier scale (Kääb et al., 2012; Bhattacharya et al., 2016, Bhushan et al., 2017; Brun et al., 2017; Bandyopadhyay et al., 2019; Maurer et al., 2019). Fig. 7 compares important previous geodetic measurements performed in the study region (Uttarakhand) which clearly shows that the MB of Dokriani is less negative than all the geodetic measurements. It is notable here that, on the regional scale, only one study (Bandyopadhyay et al., 2019) has estimated MB exclusively for the Uttarakhand. Other regional studies have included Uttarakhand in west Nepal region. When glaciers from Himachal and Nepal are included, the MB values become comparatively less negative (−0.34 m w.e. y^{-1}; Kääb et al., 2012; Brun et al., 2017) (Fig. 7). However, for Uttarakhand region only, the geodetic MB is −0.58 m w.e. y^{-1} (Bandyopadhyay et al., 2019), which is considerably higher negative than the Dokriani Glacier (Fig. 7). This entire exercise of comparison shows that the MB of the Dokriani Glacier is less negative than other regional geodetic measurements and, hence, it cannot be the representative of the region. The less negative MB of the Dokriani Glacier can be attributed to its huge accumulation area (area accumulation ratio = ~68%) (Fig. 1) which likely compensates for the mass loss in the lower tongue. For Bhagirathi basin only, Bandyopadhyay et al. (2019) estimated the MB of −0.35 m w.e. y^{-1} (Fig. 7), which, though higher than geodetic MB of Dokriani (−0.23 m w.e. y^{-1}), is comparable with its glaciological MB (−0.34 m w.e. y^{-1}).

5.3. Morphological evolution of the Dokriani Glacier

From the above discussion (sections 4.2 and4.3) it is clear that the MB of Dokriani Glacier is less negative than the regional MB. However, the Dokriani is one of high retreating glaciers of the region (Garg et al., 2017b). It is to be reiterated that the MB is a direct while snout retreat is a delayed response of the glaciers to climate change (Armstrong, 2010; Azam et al., 2018; Abdullah et al., 2020). The MB and snout retreat are often not in phase. For instance, out of 4 glaciers in Uttarakhand that were surveyed for their MB measurements, the Tipra bank (−0.14 m w.e. y^{-1}) and Dokriani (−0.33 m w.e. y^{-1}) have low rates of mass loss whereas the Chorabari (−0.73 m w.e. y^{-1}) and Dunagiri (−1.04 m w.e. y^{-1}) experienced high mass loss during their respective monitoring periods (Fig. 6; Pratap et al., 2016; Azam et al., 2018). However, the snout retreat was much higher (more than double) in the Dokriani (18.30 m y^{-1}) and Tipra bank glacier (17.78 m y^{-1}) as compared to Chorabari (7.36 m y^{-1}) and Dunagiri (6.1 m y^{-1}) during 1994–2015 (Garg et al., 2017b). Though the time period between MB and retreat measurements differs, it can be deciphered that retreat cannot be used as a proxy for MB. It is because, snout retreat is largely

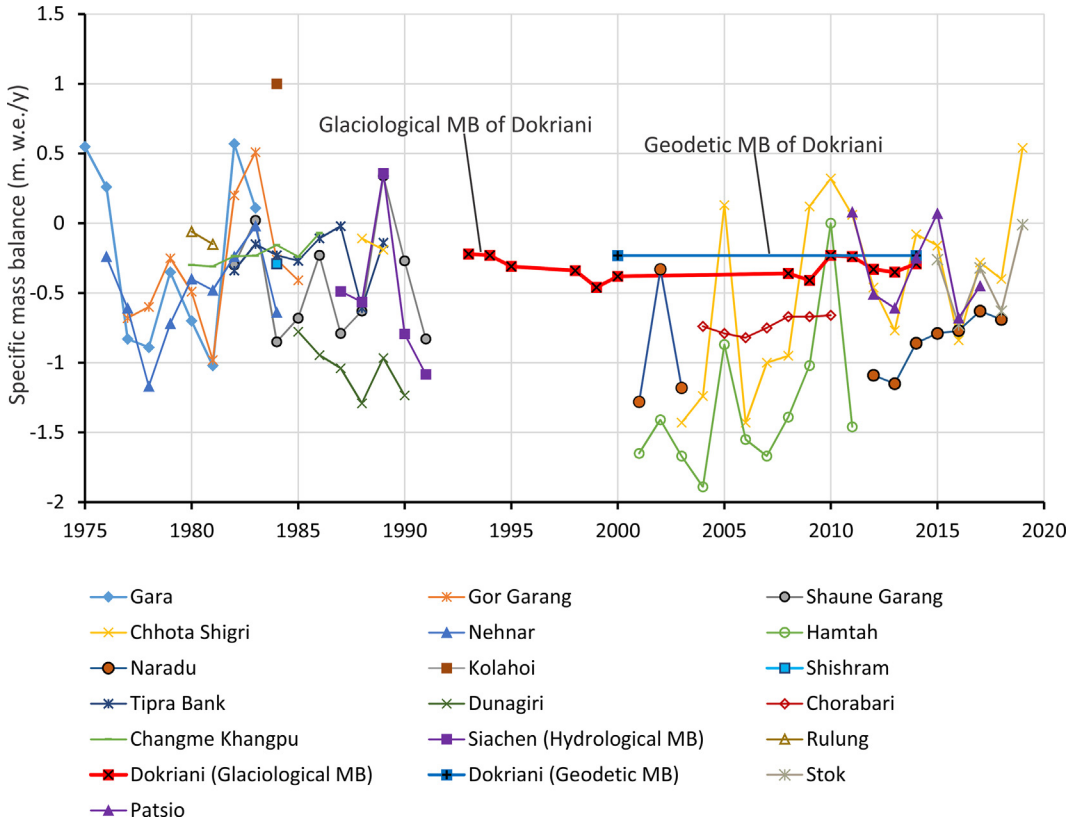

Fig. 6. Glaciological mass balance measurements in the Himalaya. Figure also shows the geodetic mass balance of the Dokriani Glacier for the comparison purpose. Notice that geodetic mass balance of the Dokriani Glacier is less negative than glaciological one.

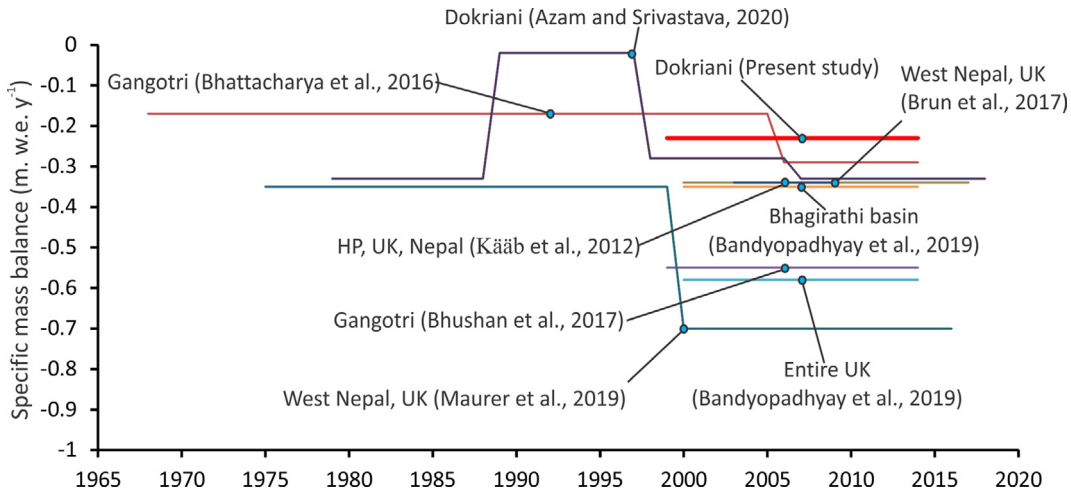

Fig. 7. Comparison of geodetic mass balance of the Dokriani Glacier to that of other geodetic measurements in the region (Uttarakhand, India, central Himalaya). Notice, the mass balance of Dokriani which is less negative than most of the other measurements and, hence, restricts it to be a representative glacier of the region. Details of references in the figure can be found in list of references given at the end of manuscript.

influenced by the terminus environment such as debris thickness, presence of proglacial lakes, lake- or dry-calving, impact of surrounding moraines or side valley walls (Armstrong, 2010; Garg et al., 2017b).

The tongue of the Dokraini glacier lies between high rising right and left moraines (Figs. 1 and 8). Usually, in the debris-covered glaciers, typical debris distribution is such that the debris thickness reduces with increasing distance from the snout towards upglacier but increases with increasing distance from central flow line towards margins (Schauwecker, 2017; Anderson and Anderson, 2018). This generalization is reaffirmed by the field measurements of debris thickness at the Dokraini glacier which shows that the central portion of the glacier is either clean or have very thin debris cover (<2–5 cm) whereas towards margins the debris is very thick

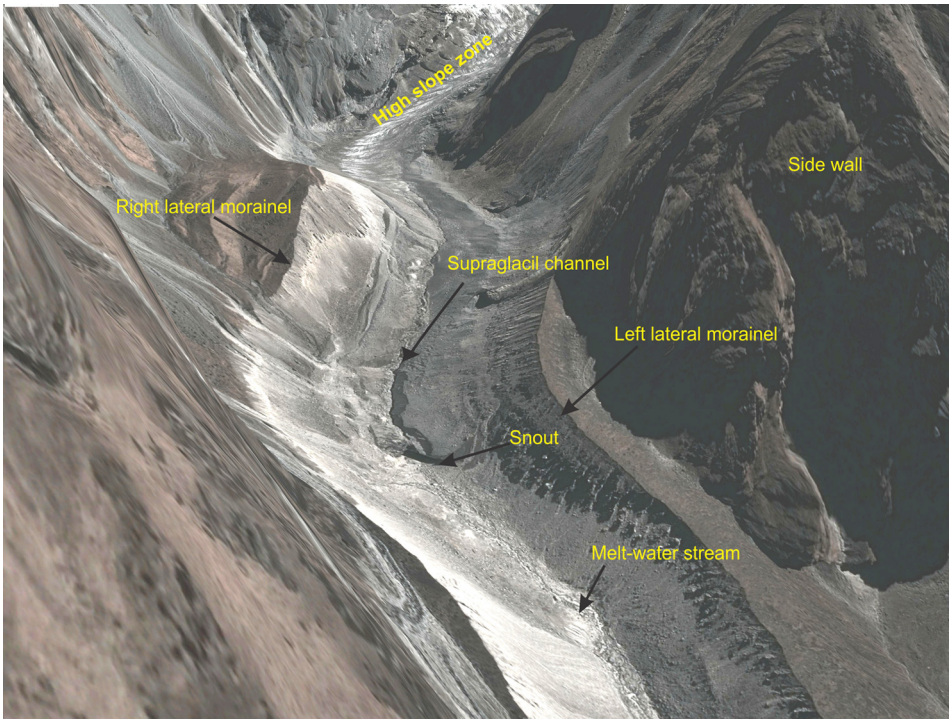

Fig. 8. Google Earth image of 2014 showing various prominent morphological features present in the lower tongue of the Dokriani Glacier.

(25–40 cm; Pratap et al., 2016). This debris thickness distribution has resulted in differential melting, i.e., maximum melting at the center (near or along center flowline) and minimum at the margins which is well-evident in the ablation stake measurements as well as in geodetic measurements (Fig. 5). A recent study by Azam and Srivastava (2020) has also observed similar phenomenon while modeling the MB of Dokriani Glacier using mass balance-runoff model. They reported MB in order of −12 to −13 m w.e. in the central portion which is almost twice than at margins (−6 to −7 m w.e.) during 1979–2018. To study the epiglacial morphology of glacier tongue more emphatically, we have created dense cross profiles of it (Fig. 5). Since it is narrow in width, the tongue of Dokriani Glacier has become concave in shape as a consequence of differential melting (Figs. 5 and 8).

It is obvious that the free flowing water follows the general slope of underlying topography. Thus, the meltwater generated at the surface of glacier tongue would have followed the concave profile and started flowing through the center of the glacier forming a supraglacial channel. Recently, Shukla and Garg (2020) have assessed surface ice velocity of the Dokraini glacier, which shows that glacier was moving with an average rate of 22.14 ± 5.8 m y^{-1} in 1993/94, which reduced only slightly to 18.08 ± 3.1 m y^{-1} in 2000/01. However, the average velocity reduced drastically to 10.53 ± 1.7 m y^{-1} in 2015/16. The sudden reduction in glacier velocity might also have contributed in formation of supraglacial channel. Field photographs affirm that the formation of supraglacial channel is quite recent (Fig. 9). There was no such supraglacial channel on the surface of Dokriani Glacier in 1995 but a well-developed channel can be seen in 2014 (Fig. 9). The appearance of this supraglacial channel and sudden change in ablation pattern of the Dokriani Glacier due to change in epiglacial morphology has also been reported earlier (Dobhal et al., 2008; Dobhal and Mehta, 2010; Pratap et al., 2016). Study of cross profiles shows the presence of supraglacial channel upto ~ 1.5 km distance from the snout towards upglacier (Fig. 5). After that the glacier surface remains no longer concave and becomes almost flat and, hence, melting is almost uniform across the glacier (Fig. 5). Melting patterns (Fig. 5), field photographs (Fig. 9) and Google earth image (Fig. 8) clearly show that the supraglacial channel is wider in upper reaches and becomes progressively narrow towards the snout. Recent field photographs (Fig. 9c, d) show that the supraglacial channel is now connected with the snout wall which causes instability and seems to be one of the likely reasons for the frequent breaking-off of ice slabs from the snout wall. With passes of time the channel is also becoming progressively deep and wide. As per Pratap et al. (2016) the channel was about 10 m deep in 2012/13. Cross profiles (Fig. 5) show that the down wasting in the center (along central flow line where supraglacial channel exists) was about 20–25 m higher than the surrounding area. Thus, the channel can also be 20–25 m deep in some places.

Gergan et al. (1999) measured the thickness of the Dokraini glacier using ground penetrating radar (GPR) and reported glacier thickness in range of 15 to 120 m. The glacier has the maximum thickness in upper reaches (>100 m) whereas thickness in the lower glacier tongue (upto one km upglacier) is 25–50 m (Gergan et al., 1999). These results are in line with our geodetic measurements, as in the snout region (upto 500 distance from snot) we found a lowering on the order of 25–30 m. Gergan et al. (1999) also reported thickness of <25 m near snout. Considering the snout retreat between 2000 and 2014, it can be estimated that about ~250 m lower tongue of glacier has been completely vanished (Garg et al., 2017b). Therefore, in this region ~25 m lowering should have occurred which is well corroborated in geodetic measurements (Fig. 5). Moreover, if we consider average thickness of ablation tongue to be 50 m and average downwasting to be 10 m between 2000 and 2014, the remaining thickness can be estimated to be 40 m. If the current pace of downwasting continues coupled with progressive deepening/widening of supraglacial channel, the

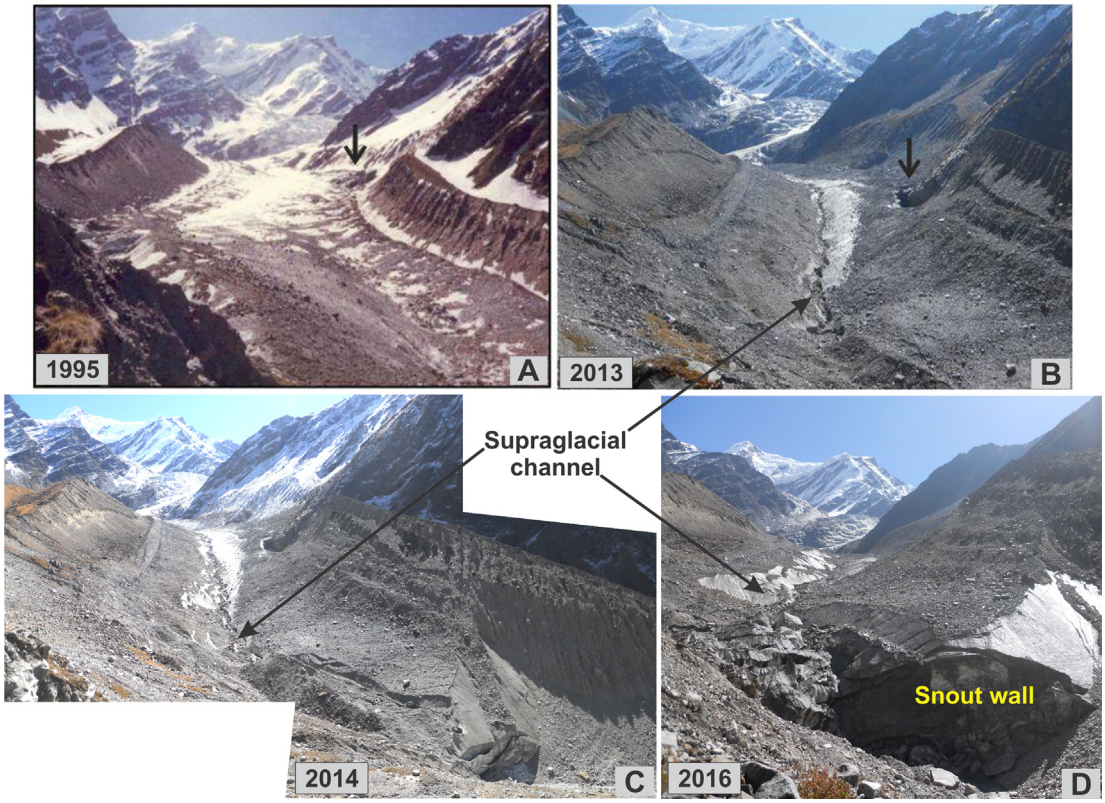

Fig. 9. Field photographs of the Dokriani Glacier for different years. Notice that no supraglacial channel was there in 1995 in the ablation tongue (Panel A). However, in 2013 a well-developed supraglacial channel can be seen clearly (Panel B). Arrows in panels (B) and (C) shows exposed rocky face due to intense down wasting of the glacier between 1995 and 2013. Panel (C) shows panoramic view of the glacier tongue created by merging two overlapping photographs that were taken from the single observation point. It is evident in the panel (C) that the supraglacial channel is connected with the snout wall and, hence, causes instability leading to rapid terminus disintegration. Panel (D) shows active disintegration of snout wall due to instable conditions. (*Source of photograph in Panel (A):* Pratap et al., 2016).

lower tongue (at least upto one km) of the Dokriani Glacier may completely vanish in coming decades.

6. Conclusions

The present study aimed at assessing the glaciological and Geodetic MB of the Dokriani Glacier for the 1999–2014 period. The study also examines the impact of prevailing MB regime on the morphological evolution of the glacier. The following major inferences can be drawn from the study.

- The MB of the Dokriani Glacier has been continuous negative during the study period of 1999–2014.
- The glaciological MB of the glacier for the year 2013/14 is -0.29 ± 0.21 m w.e. y^{-1} whereas average MB for 1999–2014 period (with intermittent gaps) is -0.34 m w.e. y^{-1}. The geodetic MB for the 1999–2014 period is -0.23 ± 0.1 m w.e. y^{-1} which is less negative than the glaciological one. Tenuous representation of margins in the glaciological MB measurements in the Dokriani Glacier, in contrast to geodetic MB where all margin (including transient) pixels are included, explains this difference.
- Rigorous comparison of MB of the Dokriani Glacier (glaciological as well as geodetic) with that of previous glacier specific and regional MB studies in the study region (Uttarakhand, central Himalaya) shows that the MB of Dokriani Glacier is less negative restricting it to be a regional representative.
- Owing to the differential debris cover, differential surface melting occurred in the glacier (i.e. maximum along central flow line and minimum at margins in lower tongue) which transformed lower tongue cross-profile into a concave one. This has eventually led to development of a supra-glacial channel in the lower glacier tongue (upto 1.5 km upglacier). The channel is progressively deepening and widening. It is now connected with the snout wall and accelerating block disintegration leading to rapid terminus retreat.
- Considering the total thickness (25–50 m) of lower tonmigue of the Dokriani Glacier, it can be said that if the current pace of downwasting continues along with progressive deepening/widening of the supraglacial channel, the lower tongue (at least upto one km) may completely vanish in coming decades.

Declaration of Competing Interest

The authors declare that they have no known competing financial interests or personal relationships that could have appeared to influence the work reported in this paper.

Acknowledgement

Authors are grateful to the Director, Wadia Institute of Himalayan Geology, Dehradun, India, for providing necessary facilities to carry out this work. A. Shukla is thankful to the Secretary, MoES for facilitating the study. P.K. Garg acknowledges the research grant from National Post-Doctoral Fellowship (NPDF) award (PDF/2020/000103) from Department of Science and Technology (DST, India). Thank is also due to U.S. Geological Survey (USGS) for providing SRTM data free of charge.

Appendix A. Supplementary data

Supplementary data to this article can be found online at https://doi.org/10.1016/j.gsf.2021.101290.

References

Abdullah, T., Romshoo, S.A., Rashid, I., 2020. The satellite observed glacier mass changes over the Upper Indus Basin during 2000–2012. Sci. Rep. 10 (1), 1–9. https://doi.org/10.1038/s41598-020-71281-7.

Agarwal, V., Bolch, T., Syed, T.H., Pieczonka, T., Strozzi, T., Nagaich, R., 2017. Area and mass changes of Siachen glacier (East Karakoram). J. Glaciol. 63 (237), 148–163. https://doi.org/10.1017/jog.2016.127.

Ahmed, N., Mahtab, A., Agrawal, R., Jayaprasad, P., Pathan, S.K., Ajai, Singh, D.K., Singh, A.K., 2007. Extraction and validation of cartosat-1 DEM. J. Indian Soc. Remote Sens. 35 (2), 121–127. https://doi.org/10.1007/BF02990776.

Anderson, L.S., Anderson, R.S., 2018. Debris thickness patterns on debris-covered glaciers. Geomorphol. 311, 1–12. https://doi.org/10.1016/j.geomorph.2018.03.014.

Andreassen, L.M., Nordli, Ø., Rasmussen, A.I., Melvold, K., Nordli, Ø., 2012. Langfjordjøkelen, a rapidly shrinking glacier in northern Norway. J. Glaciol. 58 (209), 581–593. https://doi.org/10.3189/2012JoG11J014.

Angchuk, T., Ramanathan, A., Bahuguna, I.M., Mandal, A., Soheb, M., Singh, V.B., Mishra, S., Vatsal, S., 2021. Annual and seasonal glaciological mass balance of Patsio Glacier, western Himalaya (India) from 2010 to 2017. J. Glaciol. 1–10. https://doi.org/10.1017/jog.2021.60.

Armstrong, R.L., 2010. The glaciers of the Hindu Kush-Himalayan region: a summary of the science regarding glacier melt/retreat in the Himalayan, Hindu Kush, Karakoram, Pamir, and Tien Shan mountain ranges. Int. Cent. Integr. Mt. Dev. (ICIMOD).

Azam, M.F., Srivastava, S., 2020. Mass balance and runoff modelling of partially debris-covered Dokriani Glacier in monsoon-dominated Himalaya using ERA5 data since 1979. J. Hydrol. 590, 125432. https://doi.org/10.1016/j.jhydrol.2020.125432.

Azam, M.F., Wagnon, P., Ramanathan, A., Vincent, C., Sharma, P., Arnaud, Y., Linda, A., Pottakkal, J.G., Chevallier, P., Singh, V.B., Berthier, E., 2012. From balance to imbalance: a shift in the dynamic behaviour of ChhotaShigri glacier, western Himalaya. India. J. Glaciol. 58 (208), 315–324. https://doi.org/10.3189/2012JoG11J123.

Azam, M.F., Wagnon, P., Berthier, E., Vincent, C., Fujita, K., Kargel, J.S., 2018. Review of the status and mass changes of Himalayan-Karakoram glaciers. J. Glaciol. 64 (243), 61–74. https://doi.org/10.1017/jog.2017.86.

Bandyopadhyay, D., Singh, G., Kulkarni, A.V., 2019. Spatial distribution of decadal ice-thickness change and glacier stored water loss in the Upper Ganga basin, India during 2000–2014. Sci. Rep. 9 (1), 1–9. https://doi.org/10.1038/s41598-019-53055-y.

Barnett, T.P., Adam, J.C., Lettenmaier, D.P., 2005. Potential impacts of a warming climate on water availability in snow-dominated regions. Nat. 438 (7066), 303–309. https://doi.org/10.1038/nature04141.

Benn, D.I., Bolch, T., Hands, K., Gulley, J., Luckman, A., Nicholson, L.I., Quincey, D., Thompson, S., Toumi, R., Wiseman, S., 2012. Response of debris-covered glaciers in the Mount Everest region to recent warming, and implications for outburst flood hazards. Earth Sci. Rev. 114 (1–2), 156–174. https://doi.org/10.1016/j.earscirev.2012.03.008.

Berthier, E., Arnaud, Y., Kumar, R., Ahmad, S., Wagnon, P., Chevallier, P., 2007. Remote sensing estimates of glacier mass balances in the Himachal Pradesh (Western Himalaya, India). Remote Sens. Environ. 108 (3), 327–338. https://doi.org/10.1016/j.rse.2006.11.017.

Berthier, E., Cabot, V., Vincent, C., Six, D., 2016. Decadal region-wide and glacier-wide mass balances derived from multi-temporal ASTER satellite digital elevation models. Validation over the Mont-Blanc Area. Front. Earth Sci. 4 (63), 1–16. https://doi.org/10.3389/feart.2016.00063.

Bhattacharya, A., Bolch, T., Mukherjee, K., Pieczonka, T., Kropáček, J.A.N., Buchroithner, M.F., 2016. Overall recession and mass budget of Gangotri Glacier, Garhwal Himalayas, from 1965 to 2015 using remote sensing data. J. Glaciol. 62 (236), 1115–1133. https://doi.org/10.1017/jog.2016.96.

Bhushan, S., Syed, T.H., Kulkarni, A.V., Gantayat, P., Agarwal, V., 2017. Quantifying changes in the Gangotri Glacier of Central Himalaya: evidence for increasing mass loss and decreasing velocity. IEEE J. Sel. Top Appl. Earth Obs. Remote Sens. 10 (12), 5295–5306. https://doi.org/10.1109/JSTARS.2017.2771215.

Bhushan, S., Syed, T.H., Arendt, A.A., Kulkarni, A.V., Sinha, D., 2018. Assessing controls on mass budget and surface velocity variations of glaciers in Western Himalaya. Sci. Rep. 8 (1), 1–11. https://doi.org/10.1038/s41598-018-27014-y.

Bolch, T., Pieczonka, T., Benn, D.I., 2011. Multi-decadal mass loss of glaciers in the Everest area (Nepal Himalaya) derived from stereo imagery. Cryosph. 5 (2), 349–358. https://doi.org/10.5194/tc-5-349-2011.

Bolch, T., Kulkarni, A., Kääb, A., Huggel, C., Paul, F., Cogley, J.G., Bajracharya, S., 2012. The state and fate of Himalayan glaciers. Sci. 336 (6079), 310–314. https://doi.org/10.1126/science.1215828.

Braithwaite, R.J., Konzelmann, T., Marty, C., Olesen, O.B., 1998. Errors in daily ablation measurements in northern Greenland, 1993–94, and their implications for glacier climate studies. J. Glaciol. 44 (148), 583–588.

Brun, F., Berthier, E., Wagnon, P., Kääb, A., Treichler, D., 2017. A spatially resolved estimate of High Mountain Asia glacier mass balances from 2000 to 2016. Nat. Geosci. 10 (9), 668–673. https://doi.org/10.1038/ngeo2999.

Chen, J.L., Wilson, C.R., Tapley, B.D., 2013. Contribution of ice sheet and mountain glacier melt to recent sea level rise. Nat. Geosci. 6 (7), 549–552. https://doi.org/10.1038/NGEO1829.

Cogley, J.G., Adams, W.P., 1998. Mass balance of glaciers other than the ice sheets. J. Glaciol. 44 (147), 315–325. https://doi.org/10.3189/S0022143000002641.

Cogley, J.G., Hock, R., Rasmussen, L.A., Arendt, A.A., Bauder, A., Braithwaite, R.J., Jansson, P., Kaser, G., Möller, M., Nicholson, L., Zemp, M., 2011. Glossary of glacier mass balance and related terms. IHP-VII Hydrol. Tech. Doc. 86, IACS Contribution 2. [Available online at http://unesdoc.unesco.org/images/0019/001925/192525e.pdf.]

Cox, L.H., March, R.S., 2004. Comparison of geodetic and glaciological mass-balance techniques, Gulkana Glacier, Alaska. USA. J. Glaciol. 50 (170), 363–370.

Dehecq, A., Gourmelen, N., Gardner, A.S., Brun, F., Goldberg, D., Nienow, P.W., Berthier, E., Vincent, C., Wagnon, P., Trouvé, E., 2019. Twenty-first century glacier slowdown driven by mass loss in High Mountain Asia. Nat. Geosci. 12 (1), 111–127. https://doi.org/10.1038/s41561-018-0271-9.

Dobhal, D.P., Gergan, J.T., Thayyen, R.J., 2004. Recession and morphogeometrical changes of Dokriani glacier (1962–1995) Garhwal Himalaya. India. Curr. Sci. 86 (5), 692–696.

Dobhal, D.P., Gergan, J.T., Thayyen, R.J., 2008. Mass balance studies of the Dokriani Glacier from to, Garhwal Himalaya. India. Bull. Glaciol. Res. 25, 9–17.

Dobhal, D.P., Mehta, M., 2010. Surface morphology, elevation changes and terminus retreat of Dokriani Glacier, Garhwal Himalaya: implication for climate change. Himal. Geol. 31 (1), 71–78.

Dobhal, D.P., Mehta, M., Srivastava, D., 2013. Influence of debris cover on terminus retreat and mass changes of Chorabari Glacier, Garhwal region, central Himalaya. India. J. Glaciol. 59 (217), 961–971. https://doi.org/10.3189/2013JoG12J180.

Fountain, A.G., Vecchia, A., 1999. How many stakes are required to measure the mass balance of a glacier? Geogr. Ann. Ser. A 81 (4), 563–573. https://doi.org/10.1111/1468-0459.00084.

Gardelle, J., Berthier, E., Arnaud, Y., 2012. Impact of resolution and radar penetration on glacier elevation changes computed from DEM differencing. J. Glaciol. 58 (208), 419–422. https://doi.org/10.3189/2012JoG11J175.

Gardelle, J., Berthier, E., Arnaud, Y., Kääb, A., 2013. Region-wide glacier mass balances over the Pamir-Karakoram-Himalaya during 1999–2011. Cryosph. 7 (6), 1263–1286. https://doi.org/10.5194/tc-7-1263-2013.

Garg, P.K., Shukla, A., Tiwari, R.K., Jasrotia, A.S., 2017a. Assessing the status of glaciers in part of the Chandra basin, Himachal Himalaya: a multiparametric approach. Geomorphol. 284, 99–114. https://doi.org/10.1016/j.geomorph.2016.10.022.

Garg, P.K., Shukla, A., Jasrotia, A.S., 2017b. Influence of topography on glacier changes in the central Himalaya. India. Glob. Planet. Change 155, 196–212. https://doi.org/10.1016/j.gloplacha.2017.07.007.

Garg, P.K., Shukla, A., Jasrotia, A.S., 2019. On the strongly imbalanced state of glaciers in the Sikkim, eastern Himalaya. India. Sci. Total Environ. 691, 16–35. https://doi.org/10.1016/j.scitotenv.2019.07.086.

Garg, P.K., Garg, S., Yousuf, B., Shukla, A., Kumar, V., Mehta, M., 2021. Stagnation of the Pensilungpa glacier, western Himalaya, India: causes and implications. J. Glaciol. 1–15. https://doi.org/10.1017/jog.2021.84.

Gergan, J.T., Dobhal, D.P., Kaushik, R., 1999. Ground penetrating radar ice thickness measurements of Dokriani bamak (glacier), Garhwal Himalaya. Curr. Sci., 169–173

Hock, R., Jensen, H., 1999. Application of kriging interpolation for glacier mass balance computations. Geogr. Ann. Ser. A 81 (4), 611–619. https://doi.org/10.1111/1468-0459.00089.

Huggel, C., Haeberli, W., Kääb, A., Bieri, D., Richardson, S., 2004. An assessment procedure for glacial hazards in the Swiss Alps. Can. Geotech. J. 41 (6), 1068–1083. https://doi.org/10.1139/t04-053.

Huss, M., Bauder, A., Funk, M., 2009. Homogenization of long-term mass-balance time series. Ann. Glaciol. 50 (50), 198–206. https://doi.org/10.3189/172756409787769627.

INCAA, 2010. Indian Network for Climate Change Assessment and India. Climate Change and India: A 4×4 Assessment, a Sectoral and Regional Analysis for 2030s (Vol. 2). Minist. Environ. For., Government of India, 164.

IPCC, 2013. Climate Change 2013: The Physical Science Basis. Contribution of Working Group I to the Fifth Assessment Report of the Intergovernmental Panel on Climate Change [Stocker, T.F., D. Qin, G. K. Plattner, M. Tignor, S.K. Allen, J. Boschung, A. Nauels, Y. Xia, V. Bex and P.M. Midgley (eds.)]. Cambridge University Press, Cambridge, United Kingdom and New York, NY, USA, 1535.

Jansson, P., 1999. Effect of uncertainties in measured variables on the calculated mass balance of Storglaciären. Geogr. Ann. A 81 (4), 633–642.

Kääb, A., Reynolds, J.M., Haeberli, W., 2005. Glacier and permafrost hazards in high mountains. Glob. change mt. reg. Springer, Dordrecht, 225–234.

Kääb, A., Berthier, E., Nuth, C., Gardelle, J., Arnaud, Y., 2012. Contrasting patterns of early twenty-first-century glacier mass change in the Himalayas. Nat. 488 (7412), 495–498. https://doi.org/10.1038/nature11324.

Kumar, R., Singh, S., Singh, A., Kumar, R., Singh, S., Randhawa, S.S., 2021. Surface mass balance analysis at Naradu Glacier, Western Himalaya, India. Sci. Rep. 11 (1), 1–12. https://doi.org/10.1038/s41598-021-91348-3.

Maurer, J.M., Schaefer, J.M., Rupper, S., Corley, A., 2019. Acceleration of ice loss across the Himalayas over the past 40 years. Sci. Adv. 5 (6), 1–12. https://doi.org/10.1126/sciadv. aav7266.

Muralikrishnan, S., Pillai, A., Narender, B., Reddy, S., Venkataraman, V.R., Dadhwal, V.K., 2013. Validation of Indian national DEM from Cartosat-1 data. J. Indian Soc. Remote Sens. 41 (1), 1–13. https://doi.org/10.1007/s12524-012-0212-9.

Nicholson, L., Benn, D.I., 2006. Calculating ice melt beneath a debris layer using meteorological data. J. Glaciol. 52 (178), 463–470. https://doi.org/10.3189/172756506781828584.

Nuimura, T., Fujita, K., Fukui, K., Asahi, K., Aryal, R., Ageta, Y., 2011. Temporal changes in elevation of the debris-covered ablation area of Khumbu Glacier in the Nepal Himalaya since 1978. Arct., Antarct. Alp. Res., 43(2), 246-255. 10.1657/1938-4246-43.2.246.

Nuth, C., Kääb, A., 2011. Co-registration and bias corrections of satellite elevation data sets for quantifying glacier thickness change. Cryosph. 5 (1), 271–290. https://doi.org/10.5194/tc-5-271-2011.

Ohmura, A., 2011. Observed mass balance of mountain glaciers and Greenland ice sheet in the 20th century and the present trends. Surv. Geophys. 32 (4–5), 537–554. https://doi.org/10.1007/s10712-011-9124-4.

Østrem G., Brugman M., 1991. Glacier mass-balance measurements: amanual for field and office work. Saskatoon, Sask., Environment Canada. Natl. Hydrol. Res. Inst. (NHRI Science Report 4).

Pelto, M.S., 2000. The impact of sampling density on glacier mass balance determination. Hydrol. Process., 14(18), 3215-3225. 0.1002/1099-1085 (20001230)14:18<3215: AID-HYP197>3.0.CO;2-E.

Pieczonka, T., Bolch, T., 2015. Region-wide glacier mass budgets and area changes for the Central Tien Shan between~ 1975 and 1999 using Hexagon KH-9 imagery. Glob. Planet. Change 128, 1–13. https://doi.org/10.1016/j.gloplacha.2014.11.014.

Pratap, B., 2015. Mass balance of dokriani glacier central Himalaya a model in response to climate fluctuation and debris cover. Thesis. Univ. Pet. Energy Stud. (UPES), 2015. Shodhganga http://shodhganga.inflibnet.ac.in/handle/10603/139745.

Pratap, B., Dobhal, D.P., Mehta, M., Bhambri, R., 2015. Influence of debris cover and altitude on glacier surface melting: a case study on Dokriani Glacier, central Himalaya. India. Ann. Glaciol. 56 (70), 9–16. https://doi.org/10.3189/2015AoG70A971.

Pratap, B., Dobhal, D.P., Bhambri, R., Mehta, M., Tewari, V.C., 2016. Four decades of glacier mass balance observations in the Indian Himalaya. Reg. Environ. Change 16 (3), 643–658. https://doi.org/10.1007/s10113-015-0791-4.

Quincey, D.J., Luckman, A., Benn, D., 2009. Quantification of Everest region glacier velocities between 1992 and 2002, using satellite radar interferometry and feature tracking. J. Glaciol. 55 (192), 596–606. https://doi.org/10.3189/002214309789470987.

Rignot, E., Echelmeyer, K., Krabill, W., 2001. Penetration depth of interferometric synthetic-aperture radar signals in snow and ice. Geophys. Res. Lett. 28 (18), 3501–3504. https://doi.org/10.1029/2000GL012484.

Schauwecker, S.M., 2017. Understanding climate-driven processes for data-scarce mountain glaciers: insights from reanalysis data and global climate models, as well as in-situ and remote sensing sources (Doctoral dissertation, University of Zurich). 10.5167/uzh-148761.

Scherler, D., Bookhagen, B., Strecker, M.R., 2011. Spatially variable response of Himalayan glaciers to climate change affected by debris cover. Nat. Geosci. 4 (3), 156–159. https://doi.org/10.1038/ngeo1068.

Schwitter, M.P., Raymond, C.F., 1993. Changes in the longitudinal profiles of glaciers during advance and retreat. J. Glaciol. 39 (133), 582–590. https://doi.org/10.3189/S0022143000016476.

Shroder, J.F., Bishop, M.P., Copland, L., Sloan, V.F., 2000. Debris-covered glaciers and rock glaciers in the Nanga Parbat Himalaya. Pakistan. Geogr. Ann. Ser. A 82 (1), 17–31.

Shukla, A., Garg, P.K., Srivastava, S., 2018. Evolution of glacial and high-altitude lakes in the Sikkim, Eastern Himalaya over the past four decades (1975–2017). Front. Environ. Sci. 6, 81. https://doi.org/10.3389/fenvs.2018.00081.

Shukla, A., Garg, P.K., 2020. Spatio-temporal trends in the surface ice velocities of the central Himalayan glaciers, India. Glob. Planet. Change, 190, 103187. org/10.1016/j.gloplacha.2020.103187.

Soheb, M., Ramanathan, A., Angchuk, T., Mandal, A., Kumar, N., Lotus, S., 2020. Mass-balance observation, reconstruction and sensitivity of Stok glacier, Ladakh region, India, between 1978 and 2019. J. Glaciol. 66 (258), 627–642. https://doi.org/10.1017/jog.2020.34.

Thibert, E., Blanc, R., Vincent, C., Eckert, N., 2008. Glaciological and volumetric mass-balance measurements: error analysis over 51 years for Glacier de Sarennes. French Alps. J. Glaciol. 54 (186), 522–532. https://doi.org/10.3189/002214308785837093.

Tiwari, R.K., Gupta, R.P., Arora, M.K., 2014. Estimation of surface ice velocity of Chhota-Shigri glacier using sub-pixel ASTER image correlation. Curr. Sci. 106 (6), 853–859.

Vijay, S., Braun, M., 2016. Elevation change rates of glaciers in the Lahaul-Spiti (Western Himalaya, India) during 2000–2012 and 2012–2013. Remote Sens. 8 (12), 1–16. https://doi.org/10.3390/rs8121038.

Vincent, C., Ramanathan, A., Wagnon, P., Dobhal, D.P., Linda, A., Berthier, E., Sharma, P., Arnaud, Y., Azam, M.F., Gardelle, J., 2013. Balanced conditions or slight mass gain of glaciers in the Lahaul and Spiti region (northern India, Himalaya) during the nineties preceded recent mass loss. Cryosph. 7 (2), 569–582. https://doi.org/10.5194/tc-7-569-2013.

World Glacier Monitoring Service (WGMS) Global Glacier Change Bulletin No. 2 (2014–2015) (WGMS, 2017) https://doi.org/10.5904/wgms-fog-2017-10.

Yadav, J.S., Pratap, B., Gupta, A.K., Dobhal, D.P., Yadav, R.B.S., Tiwari, S.K., 2019. Spatio-temporal variability of near-surface air temperature in the Dokriani glacier catchment (DGC), central Himalaya. Theor. Appl. Climatol. 136 (3), 1513–1532. https://doi.org/10.1007/s00704-018-2544-z.

Yadav, J.S., Misra, A., Dobhal, D.P., Yadav, R.B.S., Upadhyay, R., 2020. Snow cover mapping, topographic controls and integration of meteorological data sets in Din-Gad Basin, Central Himalaya. Quat. Int. 575, 160–177. https://doi.org/10.1016/j.quaint.2020.05.030.

Zemp, M., Thibert, E., Huss, M., Stumm, D., RolstadDenby, C., Nuth, C., Nussbaumer, S.U., Moholdt, G., Mercer, A., Mayer, C., Joerg, P.C., 2013. Reanalysing glacier mass balance measurement series. Cryosph. 7 (4), 1227–1245. https://doi.org/10.5194/tc-7-1227-2013.

Zemp, M., Frey, H., Gärtner-Roer, I., Nussbaumer, S.U., Hoelzle, M., Paul, F., Haeberli, W., Denzinger, F., Ahlstrøm, A.P., Anderson, B., Bajracharya, S., 2015. Historically unprecedented global glacier decline in the early 21st century. J. Glaciol. 61 (228), 745–762. https://doi.org/10.3189/2015JoG15J017.

Zhou, Y., Li, Z., Li, J., Zhao, R., Ding, X., 2018. Glacier mass balance in the Qinghai-Tibet Plateau and its surroundings from the mid-1970s to 2000 based on Hexagon KH-9 and SRTM DEMs. Remote Sens. Environ. 210, 96–112. https://doi.org/10.1016/j.rse.2018.03.020.